MATRIX CRACKING IN FOUR DIFFERENT 2D SiC/SiC COMPOSITE SYSTEMS

Gregory N. Morscher*
Ohio Aerospace Institute
Brookpark, OH

ABSTRACT

Silicon carbide fiber reinforced, silicon carbide matrix composites are some of the most advanced composite systems for high-temperature, high-stress applications in oxidizing environments. A basic area that needs to be understood for the purpose of material behavior modeling and optimization is the architectural, constituent, and mechanistic factors that contribute to non-linear stress-strain behavior. The mechanism that causes non-linear stress-strain in dense-matrix composites is the formation and propagation of bridged matrix cracks. In addition, the occurrence and propagation of matrix cracks controls the time-dependent strength-properties of these materials in oxidizing environments at elevated temperatures. A modal acoustic emission technique has been used to monitor and estimate the stress-dependent matrix cracking. Two different SiC matrix systems, chemical vapor infiltrated (CVI) and melt-infiltrated (MI), with two different SiC fiber reinforcement, Hi-Nicalon™ and Sylramic® were compared. Even though the averages of the range where matrix cracking occurred for the composites varied by more than 0.1% in strain and almost 200 MPa in stress, the range or distribution for matrix cracking could be reduced to a narrow band of stress for CVI SiC and MI SiC composites if it was assumed that all matrix cracks emanate outside of the load-bearing fiber, interphase, CVI SiC preform minicomposite. A simple relationship was determined to describe stress-dependent matrix cracking which can then be used to estimate the onset of large, bridged matrix cracks or for material behavior models.

INTRODUCTION: THE PROCESS OF MATRIX CRACKING IN 0/90 AND 2D WOVEN COMPOSITES

The process of matrix crack formation and growth in 2D CMC's with increasing stress has been well described [1] and for the case of cross-ply materials, effectively modeled. A brief summary of matrix cracking with increasing stress is as follows.

---

* Senior Research Scientist resident at NASA Glenn Research Center, Cleveland, OH
Work sponsored by NASA's Ultra-Efficient Engine Technology (UEET) program.

(1) *Unbridged "tunnel" crack formation*: Initial cracks occur in the 90° ply of cross-ply material [2,3] or in the 90° tows or large unbridged matrix regions of woven composites. These cracks may or may not penetrate the 0° fibers [4]. Presumably, this condition necessitates large enough flaws in the matrix to form cracks at low stresses and easy, unbridged, propagation paths for these cracks to grow (tunnel) in the composite. It should be noted, for chemical vapor infiltrated (CVI) SiC matrix composites, the first cracks occur at the sharp notches of the large continuous pores [5,6]. The cracks are stopped by the traction of 0° fibers as the crack penetrates, to a certain extent, the 0° fibers. These initial cracks in CVI SiC matrix composites form at lower stresses than 90° cracks in CVI SiC. In relatively dense matrix SiC/SiC composite, e.g., melt-infiltrated matrix, initial cracks occur for the most part in the 90° tows at significantly higher stresses than CVI matrix composites [7].

(2) *Bridged micro-crack growth*: With increasing stress, matrix cracks grow into the 0° bundles but only to a certain extent depending on the traction provided by the bridging fibers in the crack wake and the applied stress [4]. Increasing stress increases crack growth.

(3) *Through-thickness crack growth*: As stress is increased, eventually a steady-state condition is reached [8,9] where an existing tunnel-crack, "micro-crack", or newly formed crack will propagate through the thickness of the matrix resulting in a matrix crack that is fully bridged and the load in that matrix crack "plane" being fully carried by the 0° fibers. When tunnel or micro-cracks exist, some cracks may propagate through thickness, but some micro-cracks will interact with other existing, growing micro-cracks to form a continuous through thickness bridged matrix crack. In addition, some microcracks will not grow through-thickness if neighboring cracks have traversed through-thickness and are close enough so that the sliding lengths of the neighboring cracks overlap so as to cease further loading of the matrix in between the interacting neighboring matrix cracks [10].

MONITORING MATRIX CRACKING WITH MODAL ACOUSTIC EMISSION AND THE "MINIMATRIX STRESS"

For woven SiC fiber-reinforced SiC matrix composites, these three regimes of matrix crack formation and growth are observed. However, for SiC/SiC composites, measuring crack density can be very difficult especially for high modulus polycrystalline fiber composites that tend to have rougher fiber surfaces and higher interfacial shear stresses resulting in very small crack openings at stress. Also, for some composites fabricated with free silicon in the matrix, e.g., melt-infiltration (MI)*, the matrix is in compression causing matrix cracks to close. For these systems, matrix cracks can only be measured after polished sections have undergone a severe plasma etch treatment. Therefore, a modal acoustic emission (AE) technique has been developed and applied to CMC's [11-

* MI matrix composites start out the same as CVI matrix composites (see **Figure 1**): interphase CVI of a fiber preform followed by CVI of SiC. However, less CVI SiC is used for MI and the remaining open porosity is infiltrated with a SiC slurry followed by molten Si. The resulting composite usually only has a few percent of closed porosity compared to approximately 15% or greater porosity in CVI SiC matrix composites.

12] that enables the accurate location of acoustic events in the gage section of the composite tested. It has been observed that the relative cumulative AE energy is nearly proportional to the number of matrix cracks bridging load-bearing fibers. This is due to the fact that events corresponding to the formation and propagation of bridged matrix cracks are very loud compared to the other events corresponding to microcrack formation, fiber sliding, delamination, or fiber breakage and make up greater than 75% of the total cumulative energy (often this corresponds to less than 10% of the total number of events).

Figure 2 shows where the three regions of matrix cracking occur for a Sylramic-iBN, BN interphase, melt-infiltrated SiC matrix composite in relation to the stress-strain curve (**Figure 2a**) and as a function of applied stress (**Figure 2b**). *Tunnel cracking* occurs before and during the earliest detection of non-linearity in the σ/ε curve and is characterized by low-energy AE activity. Note that the inset of **Figure 2b** shows the low stress region where a greater proportion of events occur during tunnel cracking relative to the cumulative energy of the events. For that specific specimen, 108 events were detected in the 25 mm gage section prior to the occurrence of high-energy events. *Micro-crack growth* occurs just before and after the onset of detectable hysteresis loop formation and the increase in AE energy. This usually corresponds to the initial part of the "knee" in the stress-strain curve. It is difficult to quantify this region from *through-thickness crack growth*; although, this range of stress where matrix cracks do not extend through-thickness does exist. It is also of practical importance because in this *micro-crack regime* some matrix cracks do extend to the surface of the composite that may or may not result in severe strength-degradation depending on the composite system and environment. For example, when stress-rupture is performed at intermediate temperatures on specimens in this micro-crack regime for Hi-Nicalon reinforced composites (low fiber modulus, low τ, and a thin carbon layer between the fiber and the BN), crack growth occurs due to larger crack openings and preferential oxidation of the carbon layer between the fiber and the BN resulting in increasing crack opening displacement and propagation of microcracks through-thickness. In fact more AE occurs during stress-rupture for Hi-Nicalon reinforced composites than occurred during loading when tested in this stress-range. For Sylramic fiber reinforced ceramics (high fiber modulus and high τ), very little AE activity occurs after attaining the rupture load and the specimens do not fail. The retained strength of these specimens was significantly higher than the applied rupture-stress condition. Observation of the fracture surface indicates cracks that only penetrate one or two plies where oxidation of the fiber/matrix interphase had occurred, confirming that the matrix cracks were not through-thickness [13]. At some stress, *through-thickness cracking* occurs and is indicative of significant AE activity in the form of frequent high-energy events, significant hysteresis loop widths, and further non-linearity in the stress-strain curve, i.e., completion of the "knee" and further reduction in slope of the stress-strain curve with increasing stress. For most 2D woven SiC/SiC composites, the cumulative energy of AE events and the number of matrix cracks increase proportionate to increasing stress until matrix crack saturation is approached [12].

In the earlier works [14-16], the same fiber/interphase/matrix system, Sylramic/BN/MI-SiC, was compared for different 2D and 3D architectures. The final crack density (number of transverse matrix cracks per unit length) of a tensile specimen was measured after a tensile test and was multiplied to the NCumAE to estimate the

stress-dependent crack density. It was shown that for 2D and 3D architectures that possess 0/90 character, all of the matrix cracking data could be related to the stress in the matrix outside of the 0° fiber, interphase, CVI SiC minicomposite. The basis for this, as described above, is that matrix cracks originate in the 90° bundles and matrix-rich regions, including stress-risers such as sharp pores in CVI SiC. In addition, most flaws form or are propagated at stresses greater than that required to form bridged matrix cracks (Figure 1b). Therefore, based on rule of mixtures and known fractions of all the constituents in woven composites, the stress in the portion of the matrix outside of the load-bearing minicomposite could be determined. This stress was termed the "minimatrix stress" and is described as follows:

$$\sigma_{\min imatrix} = \frac{(\sigma_c + \sigma_{th})}{E_c}\left(\frac{E_c - f_{\min l} E_{\min l}}{1 - f_{\min l}}\right) \qquad [1]$$

where, σ_c is the composite stress, σ_{th} is the residual compressive stress in the matrix [17] which was found to be higher, in general, for higher volume fraction composites with inside debonding [18], and E_c is the measured composite elastic modulus from the σ/ε curve. It was shown that the distribution of matrix cracks for all the 2D and 3D composites in the Sylramic, BN, MI SiC matrix system with 0/90 structure could be described by this $\sigma_{minimatrix}$.

In this work, this concept will be carried further to different fiber and matrix systems. Specifically, two different fiber-types, Hi-Nicalon and Sylramic, and two different matrix systems, CVI SiC and MI SiC were studied. In addition, one Sylramic-MI composite was only infiltrated with Si and no SiC slurry (designated Syl- Si in Table I). Since the CVI SiC preform is the skeletal structure for all of these systems, the "minimatrix" approach could be applied in a straightforward manner.

MATRIX CRACKING IN 2D WOVEN COMPOSITES

Table I lists all the important physical and mechanical properties of the composites compared in this study. **Figure 3** shows the stress-strain behavior for the composites. In general, Sylramic fiber composites tend to have higher composite moduli and lower strains to failure compared to HN fiber composites primarily due to the higher fiber modulus and lower strain to failure of the reinforcing fiber. Also, MI composites tend to have higher stresses for the "knee" in the curve compared to CVI composites of the same fiber-type. In reference 14, the estimated crack density based on normalized cumulative AE energy (NCumAE) was determined and compared for the Sylramic, MI SiC system. This was necessary because many of the composite variations were of low fiber volume fraction and matrix crack saturation was not achieved. For the different composites compared in this study, matrix crack density varied by almost an order of magnitude depending on fiber-type and matrix (Table I). Therefore, the NCumAE behavior will be used for comparison rather than estimated crack density, i.e., when and over what stress-range matrix cracking is occurring. It is important to note that only

composites that exhibited matrix crack saturation were compared in this study. The absolute amount of stress-dependent matrix cracking could be determined by multiplying the final crack density and the NCumAE. **Figure 4a and 4b** show the NCumAE versus stress and strain for the composites tested. The range over which the different NCumAE (matrix cracking) distributions occurs is substantial. The strain ranges differ by over 0.1% and the stress ranges differ by over almost 200 MPa. This of course corresponds to the stress/strain region just prior to, during, and following the "knee" in the stress-strain curve. Two examples of matrix cracks are shown in **Figure 5** for a HN-CVI specimen and for a Syl-Sl specimen. The Syl-Sl had to be plasma-etched in order to observe matrix cracks.

Figure 6 shows the NCumAE versus $\sigma_{minimatrix}$. The data condenses down into to two distinct regions: CVI SiC matrix composites and MI matrix composites. There was more scatter for CVI SiC matrix composites with all of the stress-distributions falling within an ~ 25 MPa band of stress. For MI composites, the data was even more consistent with all of the stress-distributions falling with an ~ 12 MPa band. It is most likely that the CVI SiC data has more scatter because there is a tendency for greater variation in porosity from the edge of a panel to the center of a panel when higher CVI contents are attempted. Also, the amount of CVI SiC infiltrated into the interior of each specimen on final infiltration was not known, which could have added to the CVI SiC content in the minicomposite and thus an underestimate of f_{mini} and E_{mini}.

A simple Weibul model can be applied to best fit the NCumAE data with $\sigma_{minimatrix}$:

$$NCumAE = 1 - \exp(\phi) \qquad [2]$$

where:

$$\phi = \left(\frac{\sigma_{min\,imatrix}}{\sigma_o} \right)^m \qquad [3]$$

where σ_o, the reference stress, would correspond to the average stress of the composite system for NCumAE = 0.623. The best-fit to Equation (2) for the CVI SiC and MI SiC systems are shown in Figure 6 by the large circle data points. The σ_o values for CVI and MI composites were determined to be 118 MPa and 150 MPa, respectively. The best-fit m values for CVI and MI composites were found to be 5 and 6, respectively. Multiplying the final measured crack density (Table 1) by Equation (2) would give the stress-dependent matrix crack density.

The model-fit of the NCumAE data could then be used to also determine the onset stress for the formation of large (high AE energy) matrix cracks. A linear-regression fit of the data from Equation (2) NCumAE ranging from 0.1 to 0.9 can be performed and the line projected to zero NCumAE. The intersection of the regression fit with the abscissa of figure 6 would then estimate the minimatrix stress for the onset of large (bridged) matrix crack formation, $\sigma_{minimatrix}$ (onset). For CVI SiC composites, $\sigma_{minimatrix}$ (onset) was found to be 74 ± 13 MPa and for MI SiC matrix composites, $\sigma_{minimatrix}$ (onset) was found to be 102 ± 7 MPa.

Therefore, Equations 1-3 represent a simple, general relationship of matrix cracking in 2D CVI-SiC based composites when loaded in a fiber-direction. If one knows the processing data for a given panel or component and the saturation crack density, the absolute stress could be backed out from Equation 1 that pertains to the stress-dependent distribution of matrix cracks or $\sigma_{minimatrix}$ (onset). The stress-dependent distribution of matrix cracks is necessary for modeling stress/strain behavior [14] and for modeling intermediate temperature properties such as stress-rupture in oxidizing environments [18]. The absolute stress derived from the $\sigma_{minimatrix}$ (onset) allows a conservative estimate of the lowest applied stress-condition where time-dependent strength-degradation will occur at intermediate temperatures in oxidizing environments.

It should be noted that this analysis only applies to 2D lay-up composites with similar fiber architecture and tow size. As the number of fibers per woven tow increases, the tow width on average increases, resulting in a matrix crack distribution that is narrower with stress and is centered at a lower stress (see reference 14). In other words σ_o and m would be different. The key dimension that appears to control the $\sigma_{minimatrix}$ is the size of the smallest dimension of the 90° tow [15-16].

CONCLUSIONS

It has been demonstrated that the distribution of matrix cracks in several 2D fiber reinforced CVI SiC matrix and MI matrix composites is dependent on the stress in the matrix outside of the load-bearing fiber-interphase-CVI SiC preform minicomposite. Composites with MI SiC matrices exhibited slightly higher "minimatrix" stresses for cracking than CVI SiC matrices presumably due to the absence of sharp stress-risers in the CVI SiC matrix composites. The fiber/interphase/CVI SiC preform serves as the base skeletal structure that controls stress-dependent cracking. The relationships derived for matrix cracking are sufficient to be used by composite modelers and designers if the content of composite constituents and saturation crack density are known.

REFERENCES

1. D.S. Beyerle, S.M. Spearing, and A.G. Evans, J. Am. Ceram. Soc., 75 (12) 3321 (1992).
2. Z.C. Xia, R.R. Carr, and J.W. Hutchinson, Acta metal. mater. 41 (8) 2365 (1993)
3. Z.C. Xia and J.W. Hutchinson, Acta metal. mater 42 (6) 1933 (1994)
4. B. Cox and D.B. Marshall, J.Am.Ceram.Soc., 79 (5) 1181 (1996)
5. P. Pluvinage, A. Parvizi-Majidi, and T.W. Chou, J. Mater. Sci., 31 232 (1996)
6. L. Guillaumat and J. Lamon, Revue des composites et des materiaux avances. Vol 3., 1993 pp. 159
7. G.N. Morscher and J.Z. Gyekenesi, Ceram. Eng. Sci. Proc., 19 (3) 241 (1998)
8. J. Aveston, G.A. Cooper, and A. Kelly, The Properties of Fibre Composites, Conference Proceedings, National Physical Laboratory. IPC Science and Technology Press, Ltd., Teddington, U.K. 1971, p. 15
9. B.Budiansky, J.W. Hutchinson, and A.G. Evans, J. Mech. Phys. Solids, 34 167 (1986)

10. W.A. Curtin, J.Am.Ceram.Soc., 74 (11) 2837 (1991).
11. G.N. Morscher, Comp. Sci. Tech. 59 687 (1999).
12. G.N. Morscher, in D.O. Thompson and D.E. Chimenti, eds. Review of Progress in Quantitative Nondestructive Evaluation, CP 509, American Institute of Phisics, 2000 pp. 383
13. G.N. Morscher and J. Hurst, Ceram. Eng. Sci. Proc., 22 (3) 547 (2001)
14. G.N. Morscher, Comp. Sci. Tech. submitted
15. G.N. Morscher, H.M. Yun, and J.A. DiCarlo, J. Am. Ceram. Soc., submitted
16. G.N. Morscher, J. Am. Ceram. Soc., submitted
17. M. Steen and J.L. Valles, in M.G. Jenkins et al., eds. ASTM STP 1309, American Society for Testing and Materials, West Conshohocken, PA, 1997, p. 49.
18. G.N. Morscher, H.M. Yun, J.A. DiCarlo, L. Thomas-Ogbuji, J.Am.Ceram.Soc., in print
19. G.N. Morscher and J. D. Cawley, J. Eur. Ceram. Soc., 22 2777 (2002)

Table I: Physical and mechanical properties of composites tested.

Composite[@]	2D ; epcm[a] Weave	f_o[b]	E, GPa	σ_r[c], MPa	2f[d](BN)	2f(CVI)	f(mini)	E(mini)	ρ_c[e] #/mm
HN-MI (55)	5HS; 6.7	0.17	207	-5	0.037	0.182	0.278	305	2.3
HN-MI (157)	5HS; 5.9	0.17	205	-20	0.034	0.198	0.285	310	2.0
Syl-MI (77)	5HS; 7.1	0.17	260	-40	0.063	0.262	0.332	365	
Syl-MI (068)	5HS; 8.7	0.20	277	-67	0.076	0.299	0.384	364	10.4
Syl-MI (044)	5HS; 8.7	0.20	214	-35	0.059	0.249	0.354	369	9.5
Syl-MI (011)	5HS; 7.9	0.19	228	-57	0.076	0.244	0.354	359	10.3
Syl-MI (153)[#]	5HS; 8.7	0.20	244	-55	0.075	0.208	0.342	357	
Syl-Si	5HS; 7.9	0.18	259	-50	0.036	0.272	0.336	381	11.3
HN-CVI (015)	8HS; 6.7	0.15	200	30	0.033	0.194	0.264	312	3.1
HN-CVI (013)*	8HS; 6.7	0.12	175	10	0.094	0.219	0.279	294	
HN-CVI (016)	8HS; 6.7	0.18	222	30	0.055	0.231	0.318	306	3.2
HN-CVI (033)	5HS; 6.7	0.14	258	0	0.037	0.205	0.264	314	
HN-CVI (037)	5HS; 6.7	0.14	244	0	0.047	0.24	0.286	316	
Syl-CVI (1)	5HS; 7.9	0.18	247	--	0.069	0.441	0.438	375	10.3
Syl-CVI (2)	5HS; 7.9	0.18	254	-20	0.068	0.442	0.437	375	9.0
Syl-CVI (3)	5HS; 7.9	0.18	271	-20	0.069	0.507	0.469	378	8.1

[@] All of the composites were fabricated in part or whole by the same entity, now called General Electric Power Systems Composites, Newark DE, but in the past were owned by Dupont-Lanxide, Allied Signal, and Honeywell. The MI portion of composite fabrication was performed by Carborundum, Inc. (Niagra Falls, NY) for Syl-MI (77) and both HN-MI composites. The Si infiltration of the Syl-Si specimen was performed at NASA Glenn Research Center by Dr. R. Bhatt.

[a] HS = harness satin; epcm = tow ends per cm

[b] fraction in the loading direction only

[c] Negative (-) is compression, positive (+) is tension

[d] 2f = total volume fraction, i.e., 0° and 90° direction

[e] Crack density determined after failure.

[#] This specimen had as produced Sylramic fibers. All the other Syl composites used Sylramic fibers which had been heat-treated to form an insitu-BN layer on the surface of the fibers prior to BN interphase infiltration.

* This specimen had a carbon interphase. All other specimens had a BN interphase.

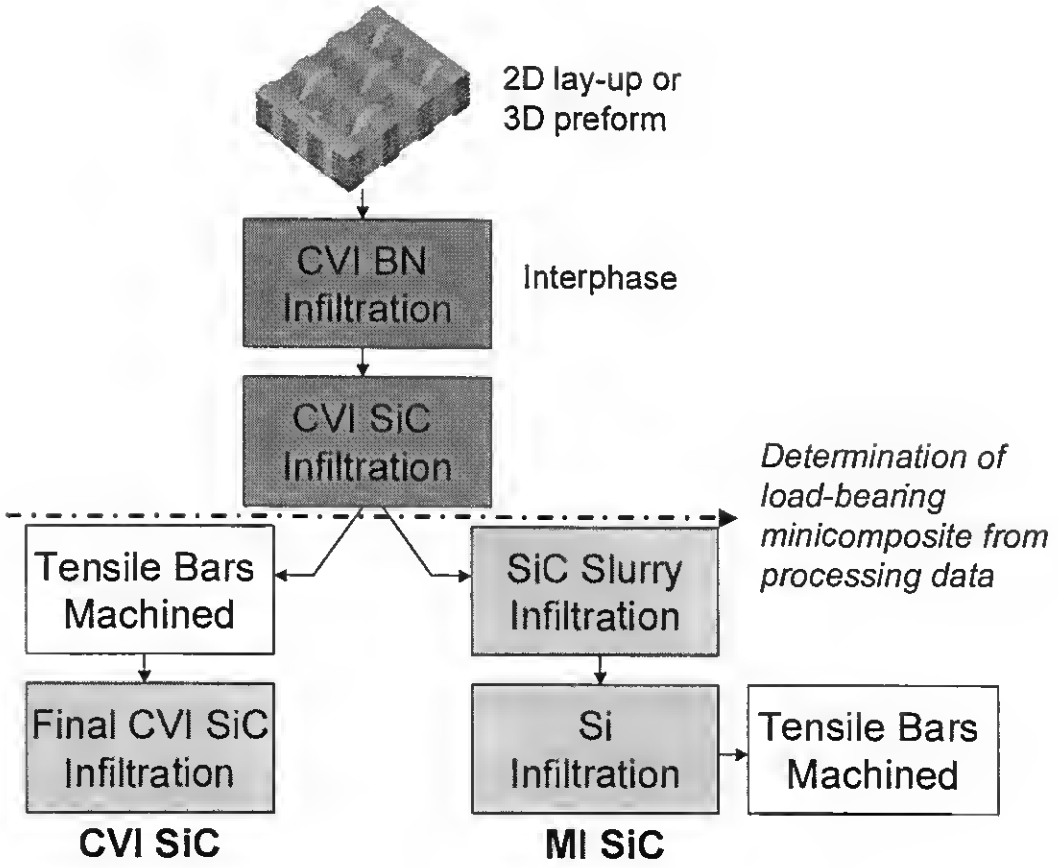

Figure 1: Schematic representation of processing steps for CVI and MI SiC composites.

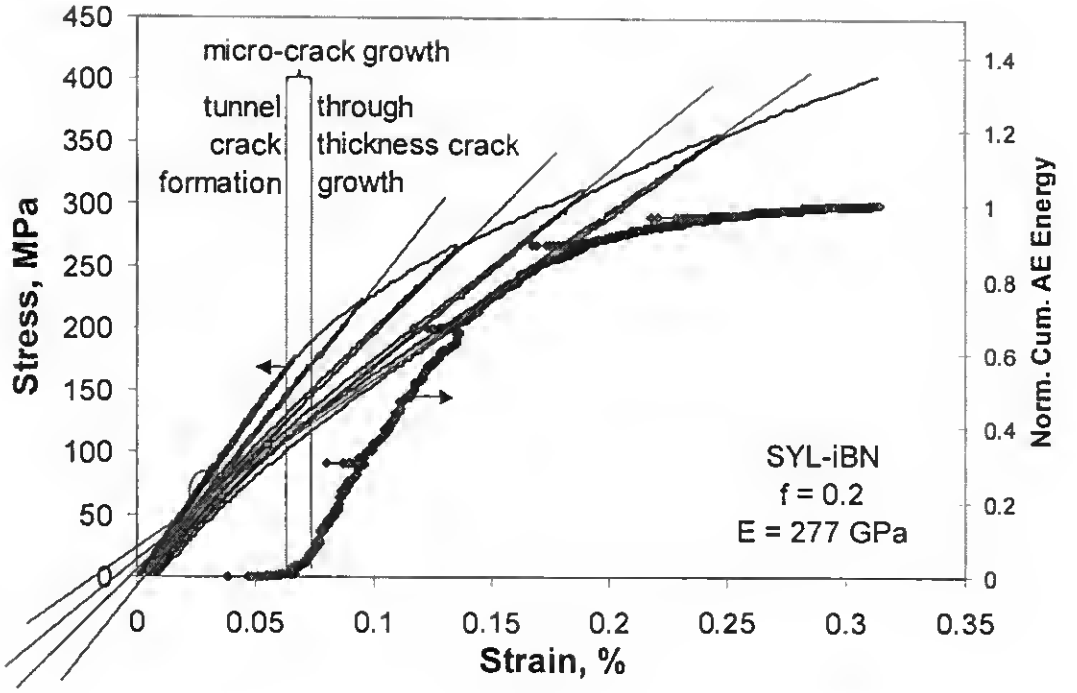

(a)

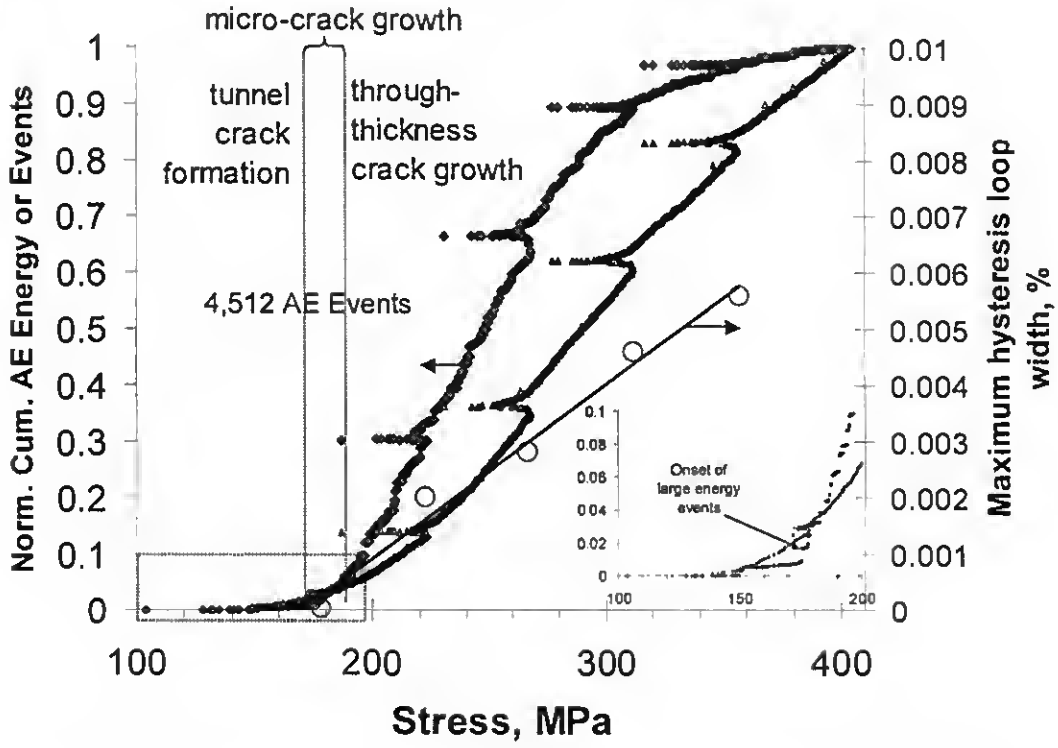

(b)

Figure 2: (a) Typical stress-strain behavior of Syl-MI composite with AE behavior. (b) AE activity versus stress. Inset in (b) corresponds to the 'boxed' low stress region.

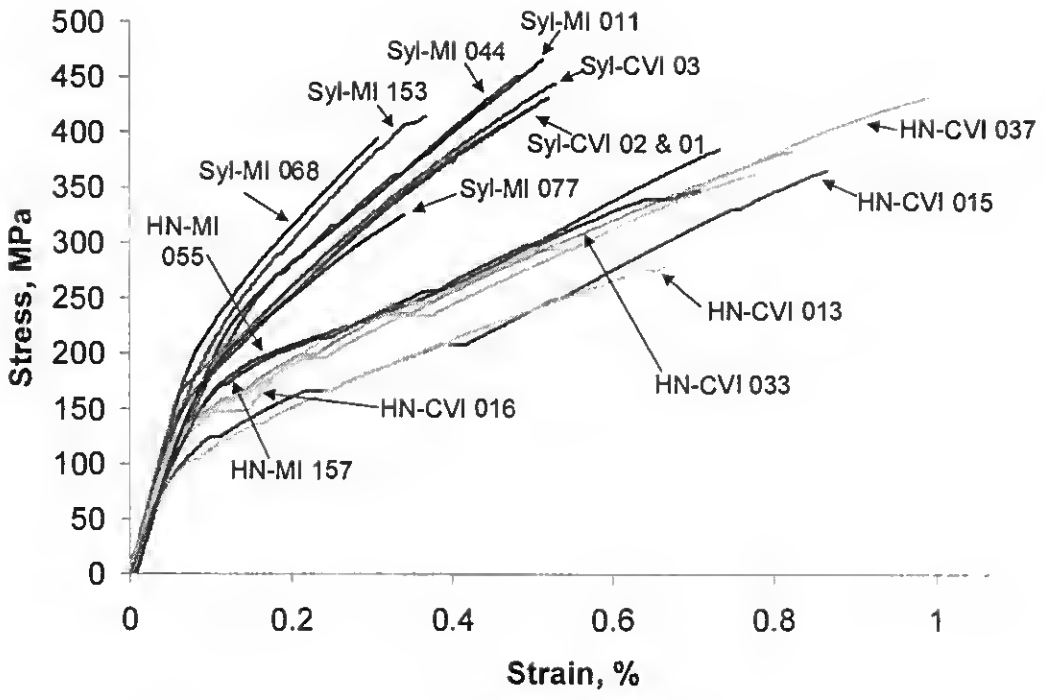

Figure 3 – Stress-strain behavior of a variety of SiC/SiC composites. Note that the hysteresis loops have been removed for clarity.

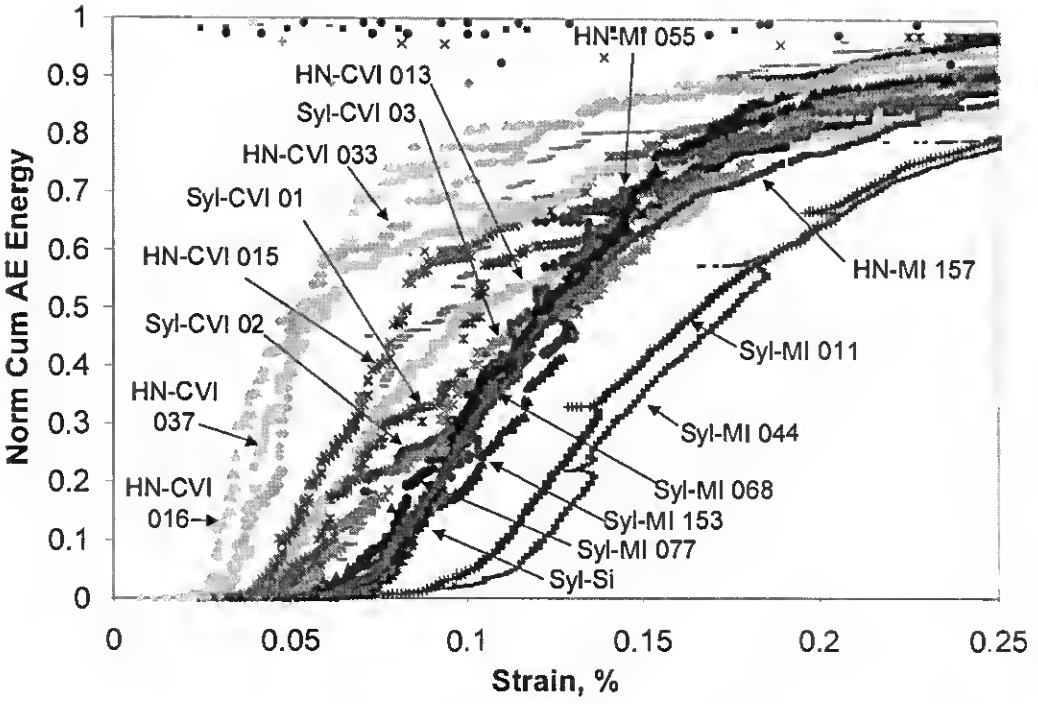

(a)

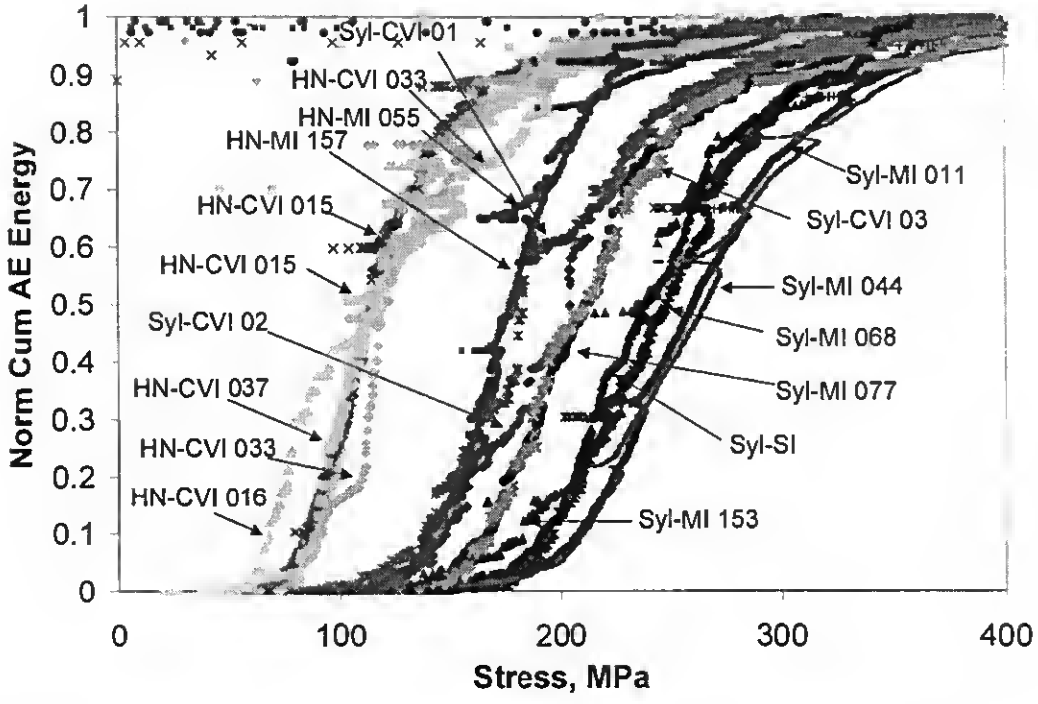

(b)

Figure 4: AE data for composites tested plotted versus (a) strain and (b) stress.

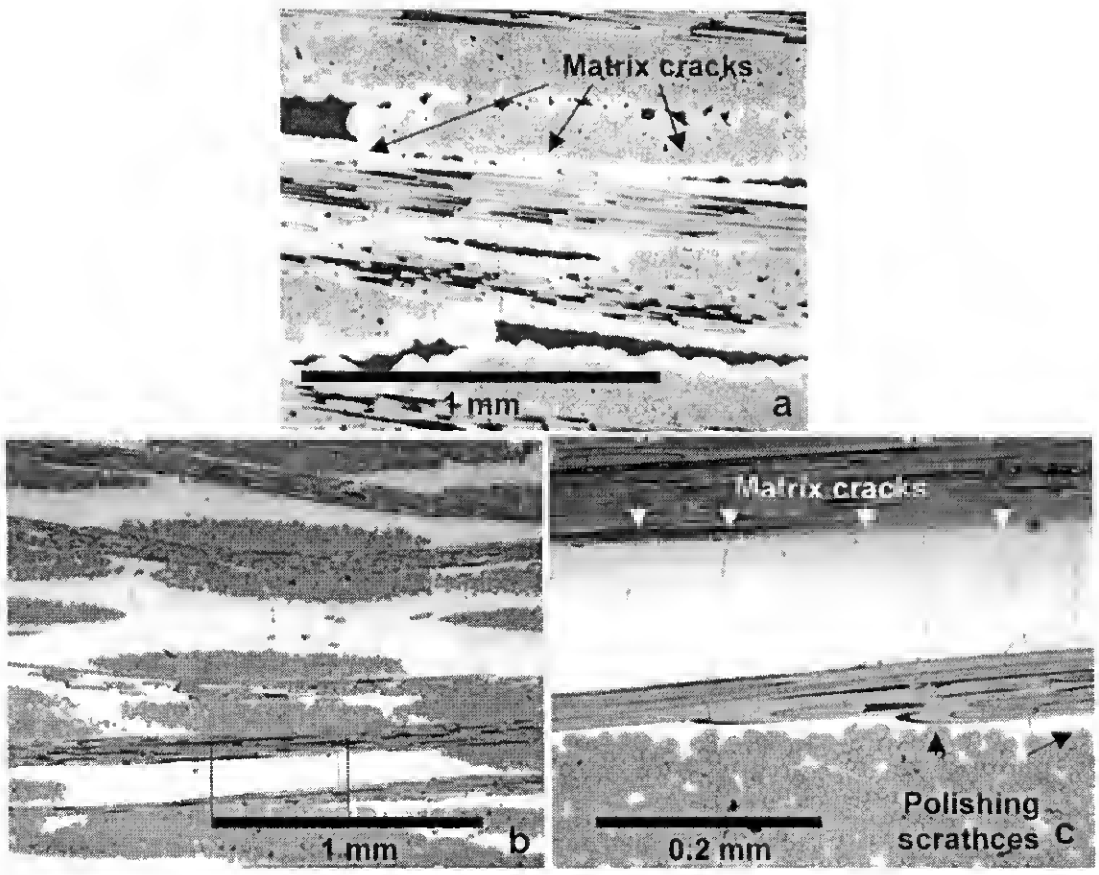

Figure 5: Examples of matrix cracks in (a) HN-CVI 015 and (b-c) Syl-SI. Note that the Syl-SI specimen was plasma-etched. Prior to plasma etching, no cracks were discernable.

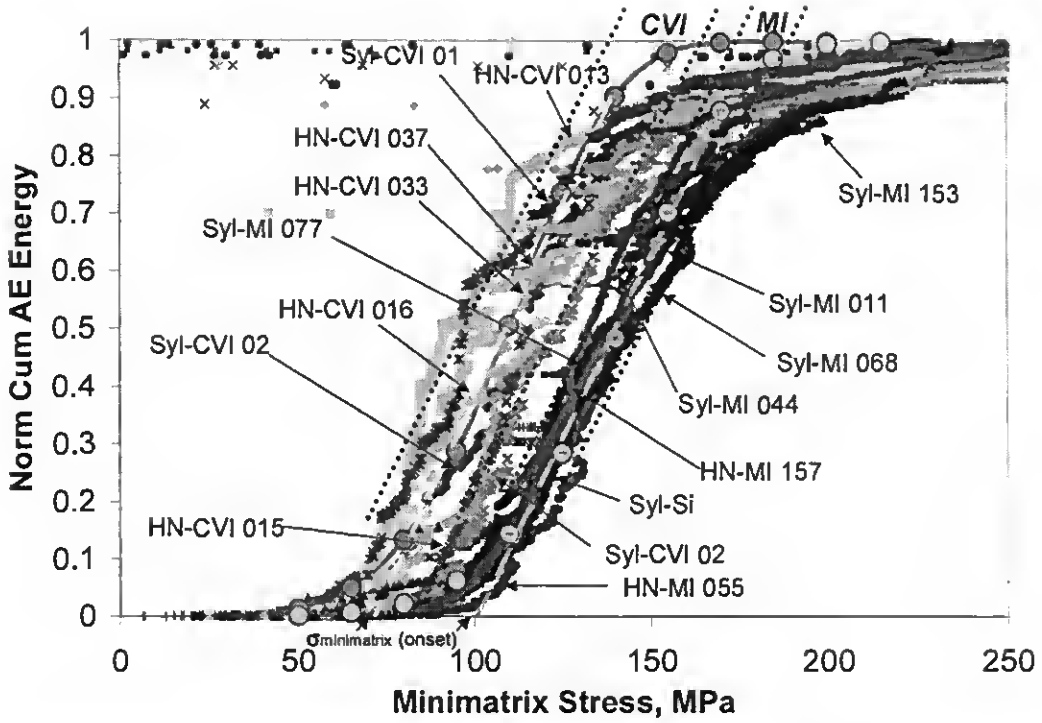

Figure 6: AE data plotted versus $\sigma_{minimatrix}$. The large circles are the model curves. The dashed lines emanating from the model-fit to the abscissa are the linear regression fit of the model data between NCumAE = 0.1 to 0.9. Where the regression fit intersects the abscissa represents the average minimatrix onset stress for large matrix crack formation.